Available online at www.sciencedirect.com
ScienceDirect
Trans. Nonferrous Met. Soc. China 26(2016) 3154−3160
Transactions of Nonferrous Metals Society of China
www.tnmsc.cn

Dynamic indentation response of porous SiC/Ti-based metallic glass composite

Ben-peng WANG[1], Lu WANG[1,2], Yun-fei XUE[1,2], Yang-wei WANG[1,2], Hai-feng ZHANG[3], Hua-meng FU[3]

1. School of Materials Science and Engineering, Beijing Institute of Technology, Beijing 100081, China;
2. National Key Laboratory of Science and Technology on Materials under Shock and Impact, Beijing 100081, China;
3. Shenyang National Laboratory for Materials Science, Institute of Metal Research, Chinese Academy of Sciences, Shenyang 110016, China

Received 24 November 2015; accepted 28 June 2016

Abstract: Porous SiC/Ti-based metallic glass composite (Ti-BMGC), a new kind of composite, has significant application prospect in the field of light armor. To evaluate the dynamic mechanical response of the composite, dynamic Vickers hardness and indentation-induced deformation behavior were investigated by comparison with that under static indentation. The dynamic hardness was measured by a modified split Hopkinson pressure bar (SHPB). The dynamic hardness is obviously greater than the static hardness. The brittleness parameter under dynamic indentation is also greater than that under static indentation. Although the dynamic indentation induced more severe deformation behavior than the static indentation, the deformation and fracture characteristics in the two loading cases are nearly the same, both exhibiting extensive cracks in the SiC phase and severe plastic deformation in the metallic glass phase.

Key words: composite; porous SiC; metallic glass; dynamic hardness; deformation behavior

1 Introduction

SiC is usually considered as an appropriate material for the application in the field of high velocity impact due to the excellent shock resistance property. However, complete brittleness makes SiC difficult to use as a single phase material [1−3]. Bulk metallic glasses (BMGs) have excellent properties, such as ultrahigh strength, high hardness, and relatively high fracture toughness. Especially, BMGs exhibit excellent energy absorption property due to large elastic strain [4−6]. Thus, the composite combining BMGs as matrix with SiC as reinforcement may further improve the shock resistance of SiC. Based on the concept referred above, porous SiC/Ti-based metallic glass composite (Ti-BMGC) with mutual reinforcement between the two phases in three-dimensional (3D) directions was developed, and the Ti-BMGC exhibited much greater fracture strength in comparison with other kinds of BMG-based composites (BMGCs) [7−9]. Thus, the Ti-BMGC may be utilized as a kind of effective armor material against ballistic threats.

Currently, indentation loading was extensively performed to model the failure behavior of the brittle materials under projectile impact [10−14]. Although the fracture mechanics under static indentation have made significant contributions to explain the fracture behavior, it could not be fully applied to analyzing the dynamic inelastic deformation behavior [15−17]. SUBHASH and ZHANG [18] reported that ZrHf-based BMG exhibited obviously lower hardness and more severe plastic deformation under dynamic indentation compared with static indentation. In contrast, compared to that under static indentation, the traditional ceramics usually exhibit greater hardness and more brittle fracture in terms of multiple cracks under dynamic indentation [16,17].

The Ti-BMGC failed earlier and exhibited lower fracture strength under high strain rate (~10^3 s^{-1}) compared to that under low strain rate (~10^{-3} s^{-1}) in uniaxial compression [8]. Similarly, the failure behavior and hardness of Ti-BMGC may also exhibit obviously different characteristics under static and dynamic indentations. Therefore, dynamic indentation technique

Foundation item: Projects (51471035, 51101018) supported by the National Natural Science Foundation of China; Project supported by the Beijing Higher Education Young Elite Teacher Project; Project supported by the Program of "One Hundred Talented People" of the Chinese Academy of Sciences

Corresponding author: Yun-fei XUE; Tel: +86-10-68912709-107; E-mail: xueyunfei@bit.edu.cn

DOI: 10.1016/S1003-6326(16)64447-3

based on a modified split Hopkinson pressure bar (SHPB) [19−21] was employed to evaluate the dynamic mechanical response of the Ti-BMGC in the present work.

2 Experimental

Ingots of $Ti_{32.8}Zr_{30.2}Cu_9Ni_{5.3}Be_{22.7}$ alloy were prepared by arc-melting the elemental metals (purity ≥99.9%) in a Ti-gettered argon atmosphere. The porous SiC was prepared by powder metallurgy. The pore distribution of the porous SiC was measured by the mercury porosimetry using the PoreMasterGT 60. The Ti-BMGC with 85% SiC (volume fraction) was prepared by pressure infiltration. The detailed description was presented in Ref. [22].

Structure characteristics of the Ti-based BMG (Ti-BMG) and Ti-BMGC were analyzed by conventional X-ray diffraction (XRD), as shown in Fig. 1. No other crystalline phases except SiC phase were detected within the sensitivity limit of XRD. The deformation and failure morphologies were examined by scanning electron microscopy (SEM).

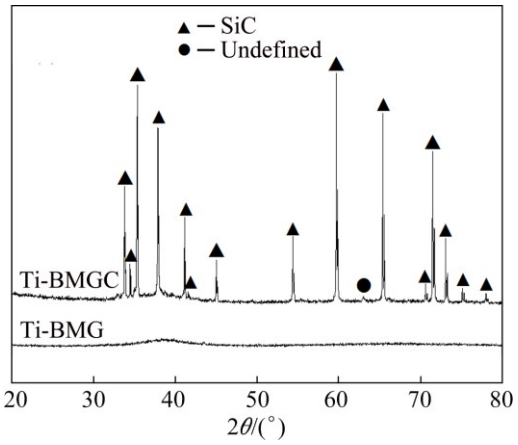

Fig. 1 XRD patterns of Ti-BMG and Ti-BMGC

A bonded interface technique was used to reveal the deformation behavior of the Ti-BMGC underneath the indentation tip. The cylindrical specimens were cut into two halves, and then the two halves were simply clamped with the polished surfaces. Details of the bonded interface technology could be found in Ref. [23].

The specimens of 5 mm in diameter and 5 mm in length were prepared for the indentation tests. Static indentations were conducted by 450SVD Vickers hardness tester. The static indentations were performed with loading duration of 10 s, thus the strain rate is typically of the order of 10^{-5} s^{-1} [19]. Dynamic indentations were performed on the self-made dynamic indentation tester, as shown schematically in Fig. 2. The equipment consists of a striker bar, an incident bar with momentum trap (MT) at one end, and a Vickers indenter with 136° face angle at the other end. The striker bar is launched from a gas gun at a predetermined velocity to impact the flange ahead of the incident bar. The impact generates both a compressive stress pulse and a tensile stress pulse, which reflect back and forth in the incident bar. However, only one compressive pulse reaches the indenter end while the rest of the stress pulses reaching the indenter end are reflected back as tensile pulse due to the MT assembly [18,19,21]. The compressive pulse drives the desired indentation while the tensile pulse retracts the indenter from the specimen, ensuring that only a single indentation event. The signal of the load history for each indentation is captured by the piezoelectricity load transducer, obtaining the indentation load data. Dynamic indentation generates a single indentation with a total duration of ~200 μs, resulting in the average strain rate in the range of 10^3−10^4 s^{-1} [19,21]. Dynamic hardness (H_d) is calculated by

$$H_d=2(P_{max}/9.8)(\sin\alpha/2)d^2=0.1892P_{max}/d^2 \quad (1)$$

where P_{max} is the peak load, N; d is the average length of the indentation diagonal, mm; α is face angle of the indenter, 136°. The flat surface was polished by SiC paper with 1500 grit and then 1.5 μm Al_2O_3 to obtain the mirror finish. Different from the static indentation, the load of dynamic indentation is difficult to control precisely due to the slight fluctuation in the velocity of the striker bar as the striker bar is launched through the barrel of the gas gun (i.e., frictional effects), leading to that the dynamic hardness is relatively discrete [21,24].

Five indentations were performed to determine the average hardness in each selected loading condition

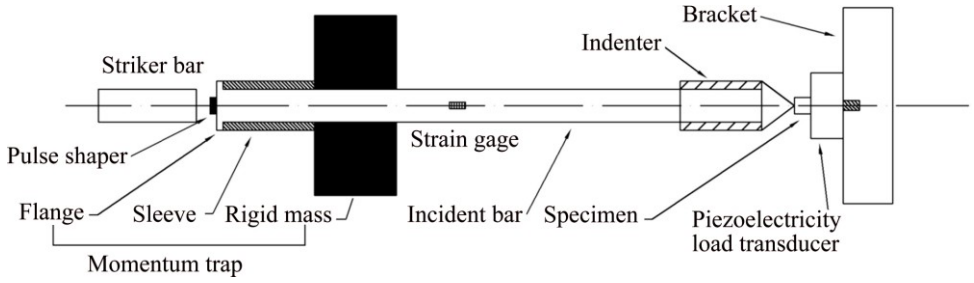

Fig. 2 Experimental setup for dynamic hardness measurement

under static indentation. During the dynamic indentation experiment, it was found that the striker bar could not be launched through the barrel of the gas gun when the load was too low; while the Ti-BMGC easily fractured into several fragments when the load was too great. Thus, to obtain the available dynamic hardness, the indentations were mainly performed under the load from 38 to 60 kg. Actually, it is still difficult to ensure that the indentation is regular even though the load is in the range of 38−60 kg because of the brittleness of Ti-BMGC. As a result, to ensure the reliability of the dynamic hardness, numerous indentations with the load from 38 to 60 kg were performed and then five of them with the most regular shape were selected to determine the dynamic hardness.

3 Results

Figure 3 shows the microstructure and the pore diameter distribution of the porous SiC. As shown in Fig. 3(a), the porous SiC exhibited a 3D interconnected net structure. The pore diameter is mainly in the range of 10−40 μm, as shown in Fig. 1(b). The metallic glass phase filled into these pores in the Ti-BMGC, leading to the diameter of the metallic glass phase much less than the characterized size of the indenter in the range of 200−300 μm. The available hardness was determined by the indentation that containing the metallic glass phase and the SiC phase.

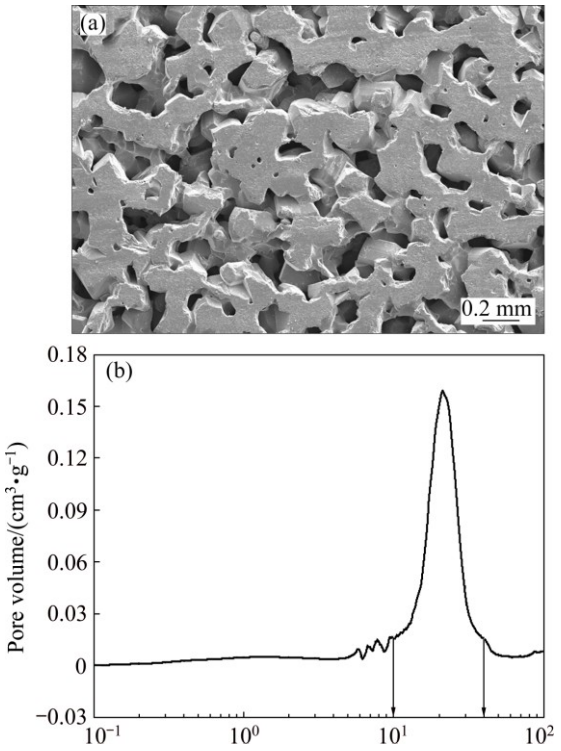

Fig. 3 Typical microstructure (a) and pore diameter distribution (b) of porous SiC

Figure 4 shows the hardness of the specimens measured under both static and dynamic indentations. Both the static and the dynamic hardness standard deviations are less than 10% of the average hardness, demonstrating that the measurement of the hardness is credible. The static hardness of the Ti-BMGC ranges from HV (1340±70) to HV (1103±95) under a load from 20 to 50 kg, whereas the dynamic hardness ranges from HV 1664 to HV 1508 under a load from 39.2 to 58.5 kg. By comparison, the dynamic hardness of the Ti-BMGC is obviously greater than the static hardness.

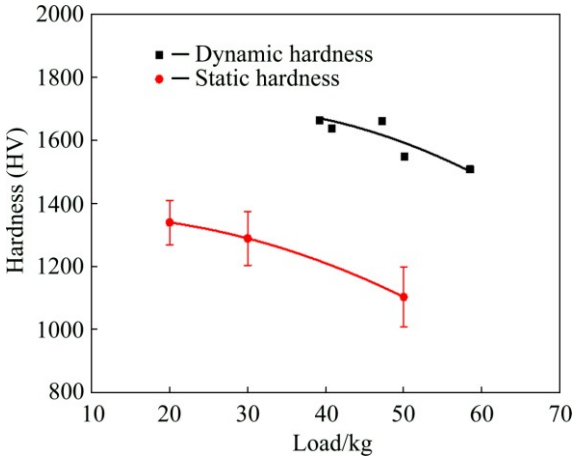

Fig. 4 Static and dynamic hardness of Ti-BMGC

To reduce the effect of loading on the mechanical behavior of the Ti-BMGC, the load under dynamic indentation (~50 kg) is as equal as that under static indentation (50 kg). Figure 5 shows the typical indentation images of the specimens on the top surface under both static and dynamic indentations. The homogeneous distribution of the grey metallic glass phase and the dark SiC phase interconnected each other in 3D directions. Typical brittle fracture in the form of extensive lateral cracks accompanied by partially developed radial cracks that emanated from the indentation corners. By contrast, the dynamic indentation induced much greater fracture (Fig. 5(b)) than the static indentation (Fig. 5(a)). Further examination of the area marked by zone I in Fig. 5(b) reveals that the cracks initiated within the SiC phase and propagated along the normal direction of the indentation corners, while no obvious cracks existed in the metallic glass phase (Fig. 5(c)). Further examination of the area marked by zone II in Fig. 5(b) reveals that multiple shear bands initiated in the metallic glass phase (Fig. 5(d)). The cracks may prefer to propagate along the interface rather than pass through the metallic glass phase, resulting in interface debonding between the two phases, as shown in Fig. 5(d).

Figure 6 shows the side morphologies of the specimens under both static and dynamic indentations.

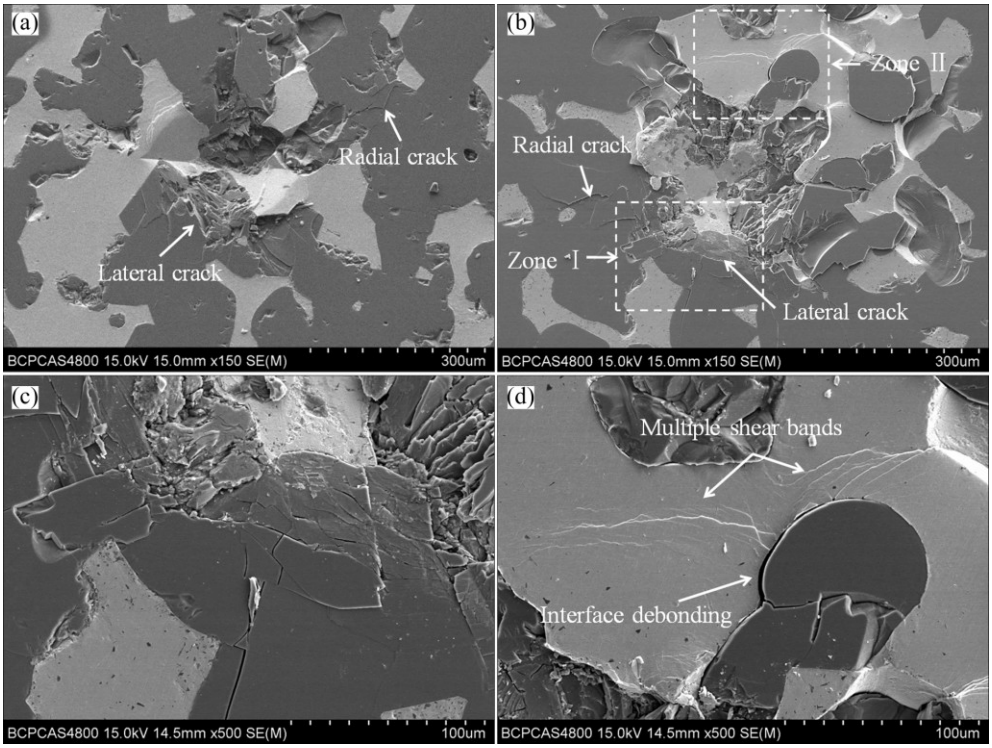

Fig. 5 SEM images of fracture regions on top surface under static indentation (a) and dynamic indentation (b), and high magnification SEM images (c, d) corresponding to zones marked by regions I and II in (b), respectively

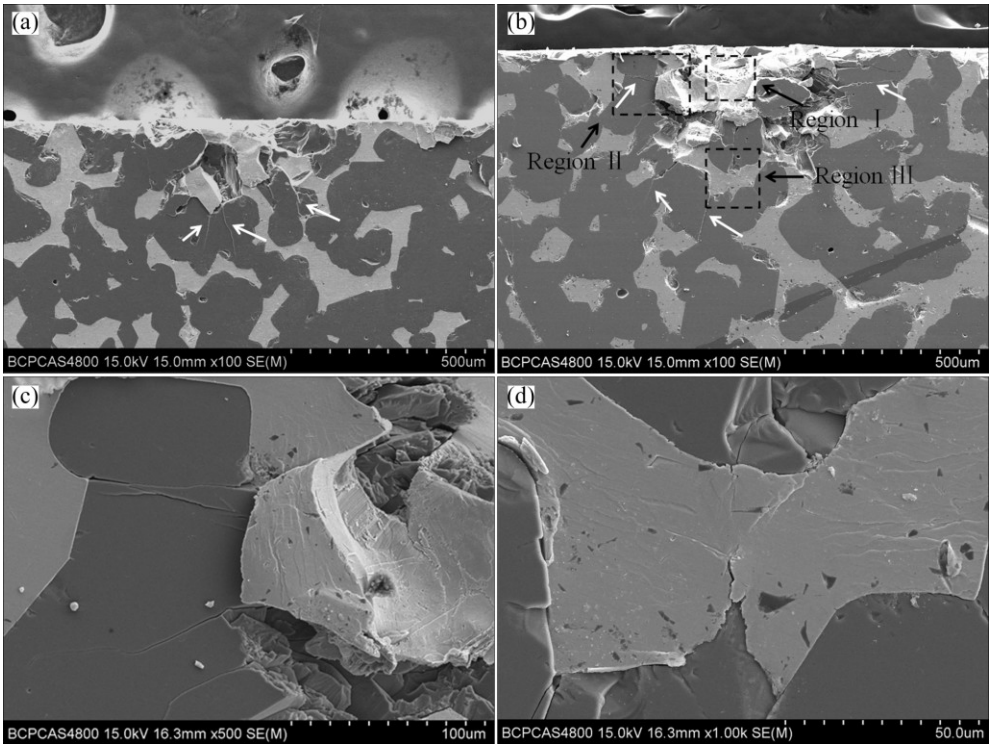

Fig. 6 SEM images of fracture regions on side surface under static indentation (a) and dynamic indentation (b), and high magnification SEM images (c, d) corresponding to zones marked by regions II and III in (b), respectively

As shown in Figs. 6(a,b), typical fracture region containing partially developed radial cracks (marked by the white arrows) formed under both the static and dynamic indentations. Compared to that only a limited number of cracks formed in the specimen subjected to static indentation (Fig. 6(a)), more cracks formed under dynamic indentation (Fig. 6(b)). The fracture region under dynamic indentation could be clearly divided into

three different regions, marked by regions I, II, and III, respectively, as shown in Fig. 6(b). Region I is close to the indentation tip, exhibiting typical brittle fracture with intense fragmentation in the two phases. Region II is in the vicinity of the indentation edge, exhibiting many macrocracks in the SiC phase but successive shear bands in the metallic glass phase, as shown in Fig. 6(c). Region III is adjacent to region I and region II, only a few macrocracks formed in the SiC phase, while successive shear bands formed in the metallic glass phase, as shown in Fig. 6(d).

4 Discussion

4.1 Strain rate dependent mechanical properties

It has been confirmed that the dynamic hardness of both SiC [15,17] and Ti-BMG [21] is obviously greater than static hardness. Therefore, the hardness enhancement of the Ti-BMGC under dynamic indentation is attributed to the strain rate dependent hardness enhancement of both the metallic glass phase and the SiC phase.

As shown in Figs. 5 and 6, the Ti-BMGC exhibits typical brittle fracture under both static and dynamic indentations. A brittleness parameter is used to measure the susceptibility of material to undergo brittle fracture, which was firstly proposed by QUINN et al [25] and subsequently revised by SUBHASH et al [24,26]. The brittleness parameter could assist in ranking of materials in terms of their ability to absorb energy. The brittleness parameter (B) was proposed by ZHANG and SUBHASH [26]:

$$B=[(EY)/\sigma_f^2)]^{1/3} \quad (2)$$

where Y is the yield strength, E is the elastic modulus, σ_f is the fracture strength. In the present work, σ_f is determined to be the fracture strength under uniaxial compression. Static yield strength of the brittle material could be estimated by the relation to static hardness proposed by ZHANG and SUBHASH [26]:

$$Y=(H^4/E)^{1/3} \quad (3)$$

where H is the static hardness. Equation (3) could also be used to calculate the dynamic yield strength. Combining Eqs. (2) and (3) gives

$$B=[(E^{2/3}H^{4/3})/\sigma_f^2]^{1/3} \quad (4)$$

Elastic modulus of the Ti-BMGC is simply calculated by the rule of mixture:

$$E=\rho_s E_s+(1+\rho_s)E_m \quad (5)$$

where ρ is the volume fraction, the subscript s and m denote SiC and Ti-BMG, respectively. Values of E_s (450 GPa) and E_m (97.8 GPa) were taken from the work of ELOMARI et al [27] and TANG et al [28], respectively. Thus, E of the Ti-BMGC is calculated to be 397.17 GPa. Table 1 lists the calculated brittleness parameters as well as the static and dynamic mechanical properties.

Table 1 Mechanical properties of present Ti-BMGC

Loading condition	E/GPa	H/GPa	σ_f/GPa [8]	B
Static	397.17	10.8	2.1	6.6
Dynamic	397.17	15.7	1.7	9.0

The brittleness parameter exhibits distinct increase under dynamic indentation compared with static indentation. It was confirmed that the higher the brittleness parameter is, the easier the brittle fracture could be induced [25,26]. Thus, the increase of the brittleness parameter could be thought as an indication of the increased tendency for the brittle fracture under dynamic indentation.

4.2 Deformation and failure behavior

The unique 3D structure of the Ti-BMGC promotes homogeneous distribution for the metallic glass phase and the SiC phase, thus the two phases deformed coordinately under the constraint of each other [7,8,22]. Due to that the SiC phase prevented the deformation of the metallic glass phase in 3D directions, the initiation and propagation of shear bands within the metallic glass phase were greatly confined, leading to that fewer successive shear bands formed within the metallic glass phase in the Ti-BMGC (Fig. 6(d)) than that in the Ti-BMG [21] at nearly the same loading cases. Thus, the metallic glass phase in the Ti-BMGC may exhibit greater hardness than Ti-BMG. On the other hand, the deformation of the SiC phase is also under the constraint of the metallic glass phase, which could obstruct the initiation and propagation of cracks in the SiC phase and lead to great hardness. Upon continuing loading, the metallic glass phase may soften due to the coalescence of free volume and adiabatic heating under high strain rate [8,29−31]. Then, the cracks within the SiC phase propagated through the metallic glass phase, as shown in Fig. 6(d). As a consequence, the mutual reinforcement of the two phases in 3D directions delayed the failure and led to great hardness for the Ti-BMGC.

5 Conclusions

1) Static and dynamic indentations were performed on the porous SiC/Ti-based metallic glass composite (Ti-BMGC). The Ti-BMGC exhibits a great hardness due to the mutual reinforcement between the two phases in three-dimensional (3D) directions.

2) Although the dynamic hardness is obviously greater than the static hardness, the deformation and fracture characteristics in the two loading cases are nearly the same except for severer deformation under dynamic indentation. Three different fracture regions were formed underneath the dynamic indentation, containing intense fragmentation in the two phases close to the indentation tip, many cracks in the SiC phase but severe plastic deformation in the metallic glass phase near the indentation edge, and slight deformation in the two phases away from the indentation tip.

References

[1] MEDVEDOVSKI E. Ballistic performance of armour ceramics: Influence of design and structure. Part 1 [J]. Ceramics International, 2010, 36: 2103−2115.

[2] MEDVEDOVSKI E. Ballistic performance of armour ceramics: Influence of design and structure. Part 2 [J]. Ceramics International, 2010, 36: 2117−2127.

[3] ERDEMIR F, CANAKCI A, VAROL T. Microstructural characterization and mechanical properties of functionally graded Al2024/SiC composites prepared by powder metallurgy techniques [J]. Transactions of Nonferrous Metals Society of China, 2015, 25: 3569−3577.

[4] ABBASI M, GHOLAMIPOUR R, SHAHRI F. Glass forming ability and mechanical properties of Nb-containing Cu−Zr−Al based bulk metallic glasses [J]. Transactions of Nonferrous Metals Society of China, 2013, 23: 2037−2041.

[5] SAEIDABADI E K, GHOLAMIPOUR R, GHASEMI B. Effect of melt infiltration parameters on microstructure and mechanical properties of tungsten wire reinforced $(Cu_{50}Zr_{43}Al_7)_{99.5}Si_{0.5}$ metallic glass matrix composite [J]. Transactions of Nonferrous Metals Society of China, 2015, 25: 2624−2629.

[6] TREXLER M M, THADHANI N N. Mechanical properties of bulk metallic glasses [J]. Progress in Materials Science, 2010, 55: 759−839.

[7] SUN Y, ZHANG H F, WANG A M, FU H M, HU Z Q, WEN C E, HODGSON P D. Mg-based metallic glass/titanium interpenetrating phase composite with high mechanical performance [J]. Applied Physics Letters, 2009, 95: 171910.

[8] WANG B P, WANG L, XUE Y F, WANG S Y, WANG Y Q, ZHANG H F, FU H M. Strain rate-dependent compressive deformation and failure behavior of porous SiC/Ti-based metallic glass composite [J]. Materials Science and Engineering A, 2014, 609: 53−59.

[9] QIAO Jun-wei. In-situ dendrite/metallic glass matrix composites: A review [J]. Journal of Materials Science and Technology, 2013, 29: 685−701.

[10] SUBHASH G, GHOSH D, BLABER J, ZHENG J Q, HALLS V, MASTERS K. Characterization of the 3-D amorphized zone beneath a Vickers indentation in boron carbide using raman spectroscopy [J]. Acta Materialia, 2013, 61: 3888−3896.

[11] IYER K A. Relationships between multiaxial stress states and internal fracture patterns in sphere-impacted silicon carbide [J]. International Journal of Fracture, 2007, 146: 1−18.

[12] NASTIC A, MERATI A, BIELAWSKI M, BOLDUV M, FAKOLUJO O, NGANBE M. Instrumented and Vickers indentation for the characterization of stiffness, hardness and toughness of zirconia toughened Al_2O_3 and SiC Armor [J]. Journal of Materials Science and Technology, 2015, 31: 773−783.

[13] LASALVIA J C, MCCAULEY J W. Inelastic Deformation mechanisms and damage in structural ceramics subjected to high-velocity impact [J]. International Journal of Applied Ceramic Technology, 2010, 7: 595−605.

[14] GAMBLE E A, COMPTON B G, DESHPANDE V S, EVANS A G, ZOK F W. Damage development in an armor ceramic under quasi-static indentation [J]. Journal of the American Ceramic Society, 2011, 94: s215−s225.

[15] GHOSH D, SUBHASH G, ZHENG J Q, HALLS V. Influence of stress state and strain rate on structural amorphization in boron carbide [J]. Journal of Applied Physics, 2012, 111: 063523.

[16] SUBHASH G, MAITI S, GEUBELLE P H, GHOSH D. Recent advances in dynamic indentation fracture, impact damage and fragmentation of ceramics [J]. Journal of the American Ceramic Society, 2008, 91: 2777−2791.

[17] KLECKA M A, SUBHASH G. Rate-dependent indentation response of structural ceramics [J]. Journal of the American Ceramic Society, 2010, 93: 2377−2383.

[18] SUBHASH G, ZHANG Hong-wen. Dynamic indentation response of ZrHf-based bulk metallic glasses [J]. Journal of Materials Research, 2007, 22: 478−485.

[19] SUBHASH G. Dynamic indentation testing [S]. ASM Handbook on Mechanical Testing and Evaluation, 2000: 519−529.

[20] ALMASRI A H, VOYIADJIS G Z. Effect of strain rate on the dynamic hardness in metals [J]. Journal of Engineering Materials and Technology, 2007, 129: 505−512.

[21] WANG B P, WANG L, XUE Y F, WANG Y W, ZHU L J, ZHANG H F, FU H M. Mechanical response of Ti-based bulk metallic glass under static and dynamic indentation [J]. Journal of Non-Crystalline Solids, 2015, 422: 32−38.

[22] CHEN Yong-li, WANG Ai-min, FU Hua-meng, ZHU Zheng-wang, ZHANG Hai-feng, HU Zhuang-qi, WANG Lu, CHENG Huan-wu. Preparation, microstructure and deformation behavior of Zr-based metallic glass/porous SiC interpenetrating phase composites [J]. Materials Science and Engineering A, 2011, 530: 15−20.

[23] XIE S, GEORGE E P. Hardness and shear band evolution in bulk metallic glasses after plastic deformation and annealing [J]. Acta Materialia, 2008, 56: 5202−5213.

[24] HANEY E J, SUBHASH G. Rate sensitive indentation response of a coarse-grained magnesium aluminate spinel [J]. Journal of the American Ceramic Society, 2011, 94: 3960−3966.

[25] QUINN J B, QUINN G D. Indentation brittleness of ceramics: A fresh approach [J]. Journal of Materials Science, 1997, 32: 4331−4346.

[26] ZHANG W, SUBHASH G. An elastic-plastic-cracking model for finite element analysis of indentation cracking in brittle materials [J]. International Journal of Solids and Structures, 2001, 38: 5893−5913.

[27] ELOMARI S, SKIBO M D, SUNDARRAJAN A, RICHARDS H. Thermal expansion behavior of particulate metal-matrix composites [J]. Composites Science and Technology, 1998, 58: 369−376.

[28] TANG M Q, ZHANG H F, ZHU Z W, FU H M, WANG A M, LI H, HU Z Q. TiZr-base bulk metallic glass with over 50 mm in diameter [J]. Journal of Materials Science and Technology, 2010, 26: 481−486.

[29] BRUCK H A, ROSAKIS A J, JOHNSON W L. The dynamic compressive behavior of beryllium bearing bulk metallic glasses [J]. Journal of Materials Research, 1996, 11: 503−511.

[30] ZHAO Ming, LI Mo. Local heating in shear banding of bulk metallic glasses [J]. Scripta Materialia, 2011, 65: 493−496.

[31] CHEN Ming-wei. Mechanical behavior of metallic glasses: Microscopic understanding of strength and ductility [J]. Annual Review Materials Research, 2008, 38: 445−469.

多孔 SiC/Ti 非晶合金复合材料的动态压痕响应行为

王本鹏[1]，王 鲁[1,2]，薛云飞[1,2]，王扬卫[1,2]，张海峰[3]，付华萌[3]

1. 北京理工大学 材料学院，北京 100081；
2. 北京理工大学 冲击环境材料技术国家级重点实验室，北京 100081；
3. 中国科学院 金属研究所沈阳材料科学国家实验室，沈阳 110016

摘 要：多孔 SiC/Ti 基非晶合金复合材料作为一种新型的复合材料，在轻质装甲领域具有重要的应用前景。通过对比研究该复合材料在静态和动态加载下的硬度和相应的压痕变形特征，揭示该复合材料的动态响应行为，评估其冲击性能，其中动态硬度采用自主设计的基于分离式霍普金森压杆(SHPB)的改进装置进行测试。研究发现复合材料的动态硬度明显高于静态硬度，其动态脆性参数也明显高于静态脆性参数。该复合材料在静态和动态加载下的变形和断裂特征并无显著差别，均表现为 SiC 相中形成了大量的裂纹而非晶相发生了剧烈的塑性变形，所不同的仅是动态压痕加载下的变形行为比静态更剧烈。

关键词：复合材料；多孔 SiC；非晶合金；动态硬度；变形行为

(Edited by Yun-bin HE)